

Dye



UNIVERSITI
TEKNOLOGI
MARA

University Publication Centre (UPENA)

Journal of Mechanical Engineering

An International Journal

Volume 7 No. 2

December 2010

ISSN 1823-5514

Modelling of Belt-Driven High-Speed Laser Beam Manipulator

Muhammad Azmi Ayub
Pavel Hynek
Mike Jackson

Computational Analysis on Thermal Performance and Coolant Flow of An Air-Cooled Polymer Electrolyte Membrane Fuel Cell

W.A. Najmi W. Mohamed
Rahim Atan

The Prediction of Transmission Loss Using Transfer Matrix Method

M. A. Yunus
A. A. Mat Isa
Z. A. Rahman
Hayder M. A. Ali Al-Assadi

The Effect of EFI to the Carbureted Single Cylinder Four Stroke Engine

Idris Ibrahim
Adibah Abdul Jalil
Shaharin A. Sulaiman

Parametric Study of Heat Transfer Enhancement Using Impingement of Multiple Air Jets

Niranjan Murthy
V. Krishnan
A. Chennakesava Reddy

Springback Analysis of Thin Tubes Under Torsional Loading

Vikas Kumar Choubey
Mayank Gangwar
J. P. Dwivedi

JOURNAL OF MECHANICAL ENGINEERING (JMechE)

EDITORIAL BOARD

EDITOR IN CHIEF:

Prof. Wahyu Kuntjoro – Universiti
Teknologi MARA, Malaysia

EDITORIAL BOARD:

Prof. Abdul Rahman Omar – Universiti
Teknologi MARA, Malaysia

Dr. Ahmad Azlan Mat Isa – Universiti
Teknologi MARA, Malaysia

Prof. Ahmad Kamal Ariffin Mohd Ihsan –
UKM Malaysia

Dr. Bambang K Hadi – Bandung Institute of
Technology, Indonesia

Prof. Dr.-Ing. Bernd Schwarze – University
of Applied Science, Osnabrueck,
Germany

Dr. Darius Gnanaraj Solomon – Karunya
University, India

Dr. Faqir Gul – Institut Technology Brunei,
Brunei Darussalam

Prof. Habil Bodo Heimann – Leibniz
University of Hannover Germany

Dr. Ichsan S. Putra – Bandung Institute of
Technology, Indonesia

Dato' Prof. Mohamed Dahalan Mohamed
Ramli – Universiti Teknologi MARA,
Malaysia

Prof. M. Nor Berhan – Universiti Teknologi
MARA, Malaysia

Professor Miroslaw L Wyszynski –
University of Birmingham, UK

Datuk Prof. Ow Chee Sheng – Universiti
Teknologi MARA, Malaysia

Prof. P. N. Rao, University of Northern
Iowa, USA

Dr. Rahim Atan – Universiti Teknologi
MARA, Malaysia

Prof. Shah Rizam Mohd Shah Baki –
Universiti Teknologi MARA, Malaysia

Dr. Talib Ria Jaffar – SIRIM Malaysia

Dr. Wirachman Wisnoe – Universiti
Teknologi MARA, Malaysia

Dr. Thomas Ward – Universiti Teknologi
MARA, Malaysia

Dr. Yongki Go Tiauw Hiong – Nanyang
Technical University, Singapore

Prof. Yongtae Do – Daegu University, Korea

EDITORIAL EXECUTIVE:

Dr. Koay Mei Hyie

Azlin Mohd Azmi

Baljit Singh

Mohamad Mazwan Mahat

Rosnadiyah Bahsan

Copyright © 2010 by the Faculty of Mechanical Engineering (FKM), Universiti Teknologi MARA, 40450 Shah Alam, Selangor, Malaysia.

All rights reserved. No part of this publication may be reproduced, stored in a retrieval system, or transmitted in any form or any means, electronic, mechanical, photocopying, recording or otherwise, without prior permission, in writing, from the publisher.

Journal of Mechanical Engineering (ISSN 1823-5514) is jointly published by the Faculty of Mechanical Engineering (FKM) and Pusat Penerbitan Universiti (UPENA), Universiti Teknologi MARA, 40450 Shah Alam, Selangor, Malaysia.

The views, opinions and technical recommendations expressed herein are those of individual researchers and authors and do not necessarily reflect the views of the Faculty or the University.

Journal of Mechanical Engineering

An International Journal

Volume 7 No. 2

December 2010

ISSN 1823-5514

1. Modelling of Belt-Driven High-Speed Laser Beam Manipulator 1
Muhammad Azmi Ayub
Pavel Hynek
Mike Jackson
2. Computational Analysis on Thermal Performance and Coolant Flow of An Air-Cooled Polymer Electrolyte Membrane Fuel Cell 15
W.A. Najmi W. Mohamed
Rahim Atan
3. The Prediction of Transmission Loss Using Transfer Matrix Method 37
M. A. Yunus
A. A. Mat Isa
Z. A. Rahman
Hayder M. A. Ali Al-Assadi
4. The Effect of EFI to the Carbureted Single Cylinder Four Stroke Engine 53
Idris Ibrahim
Adibah Abdul Jalil
Shaharin A. Sulaiman
5. Parametric Study of Heat Transfer Enhancement Using Impingement of Multiple Air Jets 65
Niranjana Murthy
V. Krishnan
A. Chennakesava Reddy

6. Springback Analysis of Thin Tubes Under Torsional Loading

81

Vikas Kumar Choubey

Mayank Gangwar

J. P. Dwivedi

Computational Analysis on Thermal Performance and Coolant Flow of An Air-Cooled Polymer Electrolyte Membrane Fuel Cell

*W.A. Najmi W. Mohamed
Rahim Atan
Alternative Energy Research Centre
Faculty of Mechanical Engineering
Universiti Teknologi MARA
Malaysia*

ABSTRACT

Polymer Electrolyte Membrane (PEM) fuel cells are electrochemical power generators that converts the energy potential of a hydrogen-based fuel into electricity with water and heat as the major by-products. The sensitivity of the solid polymer membrane to temperature requires that thermal management of a PEM fuel cell stack operates efficiently to maintain the temperature at the optimal level. Air cooling is normally applied for industrial PEM fuel cells of up to 2 kW power output. A computational investigation on the effective micro cooling channel geometries was conducted in order to enhance the practical capability of air cooling for a 3 kW stack power output with a reduced conversion efficiency of 30%. Plate and stack assembly simulation cases of a single channel and 40 cooling channel configurations using Computational Fluid Dynamics (CFD) were conducted with constant heat generation. The cooling performance was evaluated based on the boundary heat transfer and shows 100% effectiveness when subjected to air flows with a minimum Reynolds number of 200. The temperature distribution of the stack showed significant temperature gradients exists across the stack where multiple cooling channels provided a reduced gradient, approximately 50% less compared to the single channel. The coolant flow characteristics were also analyzed and an average velocity rise factor (AVRF) was introduced. Validation of the CFD simulation

results was performed analytically and the simulation methodology reliability was found satisfactory by comparing the results of single plate simulations to the stack simulations.

Keywords: *Polymer Electrolyte Membrane, fuel cells, air cooling, temperature distribution, cooling performance.*

Introduction

Green technology is an essential aspect in the modern day pursuit of quality living. Since the middle 1990s, the promising prospect of hydrogen fuel cells as a clean energy system solution has been realized with billions spent globally to develop the technology efficiently. Developed nations such as Japan, USA, Germany and Canada have led the way on the advances in fuel cell research, development and application. Green and sustainable fuel cell systems are being slowly, but surely, introduced into the mainstream applications, such as the successful residential fuel cell power system in Japan, the Honda FCX and the two-seater Peugeot Quark cars, the Formula Zero go-kart racing, and even in military applications such as night goggles and mobile power units [1].

A hydrogen fuel cell generates electricity by reversing the electrolysis process of reduction and oxidation. A hydrogen-based fuel is electrochemically split into protons and electrons by a catalyst, and the ions are channeled through separate pathways that lead to electrical current generation. These ions are then combined with oxygen that also acts like a magnet to the conductive and diffusive ionic flows, forming water molecules with a by-product of heat energy. The simplicity of the process allows a fuel cell to operate at conversion efficiencies much higher than fossil fuel power cycles. The theoretical maximum thermodynamic efficiency [2] based on the Lower Heating Value of hydrogen is approximately 83% compared to 40% for gas turbines, steam turbines, as well as diesel engines. Operating efficiencies of 40% to 50% are normally reported for hydrogen fuel cells [3], and is usually related to operating temperatures.

Though the fuel cell efficiency is proven, the issues of system durability, cost effectiveness, power-to-weight ratio as well as fuel logistics have slowed the anticipated wide scale application of hydrogen fuel cells. One of the major technical areas related to Membrane Electrode Assembly (MEA) durability is the thermal management. Widely applied technology in Polymer Electrolyte Membrane (PEM) fuel cells has low operating temperature limits, typically in the range of 60°C to 100°C [4], with MEA operating at 120°C has also been reported by Bonville et al. [5], and between 140°C to 180°C by Scholta et al. [6]. Effective thermal management is therefore necessary to maintain the operation at the desired operating temperature and maintaining a uniform cell temperature distribution [7,8]. In their work, Meyer and Yao [9] stressed that dynamic

operational thermal control of a PEM fuel cell is also important to accomplish attractive power densities and fuel-saving behavior.

Operating temperatures of a PEM fuel cell is governed by the temperature limit of the MEA. Though higher operating temperature increases the kinetics of electrochemical reactions at the Gas Diffusion Layer (GDL), excessive heat would cause unwanted thermal effects to the fuel cell. Figure 1 demonstrates the general link of thermal effect on the components and operation of a PEM fuel cell.

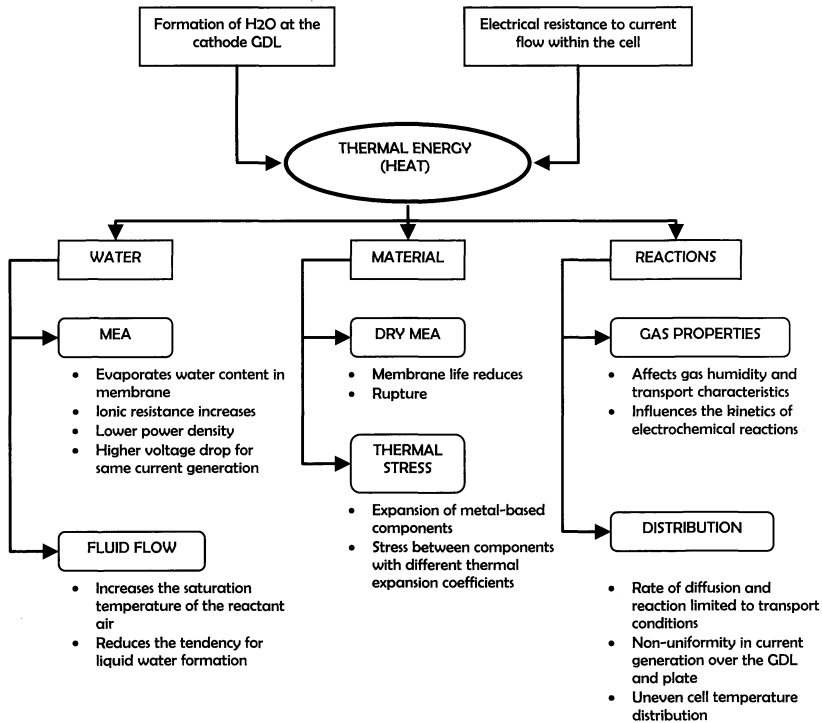


Figure 1: Generalized Thermal Effects to Fuel Cell Operation

Air Cooling of a Pem Fuel Cell

Air cooling is widely used for fuel cell stacks lower than 2 kW power rating [10]. The main technical reason is limitation in available cooling surfaces to accommodate higher cooling loads without resorting to high powered cooling fans that increases the parasitic load of the system, as well as integration of enhanced cooling surfaces that reduces the power-to-weight ratio. Normally,

air-cooled 1 kW stacks are connected in series to form an air-cooled fuel cell system with high power ratings. The commercial availability of single air-cooled stacks is limited to 5 kW with the maximum efficiency rated at 1.6 kW [11].

In order to develop an air-cooled PEM fuel cell stack for higher power ratings, two fundamental research approaches were identified. The first approach is based on the micro cooling channel designs for optimization of internal convection cooling, and secondly, at the stack and fan configuration level for enhanced overall cooling effects. The typical air cooling channel design for a closed-cathode PEM fuel cell is the integrated plate and channel design. It has the advantage of allowing a compact stack design, leading to greater mobility and suitability for low range and remote applications. At power outputs between 100 W and 1 kW, the integrated plate and channel design is more than capable to dissipate the generated heat. However, substantial bipolar plate thickness is needed to accommodate the cooling channels.

An effective fuel cell cooling system not only removes the generated heat from the stack, but is also capable of promoting a uniform temperature distribution. C.Y. Wen et al. [12] noted that none of the direct cooling methods using air and water agents is capable to homogenize the temperature inside a PEM fuel cell unit. Their work on pyrolytic graphite sheets as heat spreaders showed a better stack temperature distribution, leading to maximum power obtained 15% higher when compared to cooling without the sheets. Our previous work [13] has also identified that temperature uniformity of a fuel cell plate is difficult to achieve by air cooling. Even though the simulation of a 60 micro cooling channel configuration achieved an average plate temperature lower than operational requirements, detail analysis on the plate surfaces showed that approximately 40% of local surface temperature is actually higher than required. The highest temperatures are found at the plate edges farthest from the coolant inlet plane, with a maximum difference to the coolest region of nearly 20°C.

In order to optimize air cooling for PEM fuel cells, the geometrical and configuration effects of the cooling channels on the cooling performance and temperature distribution were investigated. The works presented here reports the thermal-fluid analysis based on computational simulation of two cooling channel configurations; a single channel and a 40 channel straight path configurations. Both configurations are fitted on a fixed bipolar plate size which is based on an industrial 3 kW water-cooled stack. Analytical comparison on its cooling performance, temperature distribution, air velocity and pressure variations based on computational simulation using Computational Fluid Dynamics (CFD) codes are conducted as a platform for practical work. Validation of the simulation results were performed by analytical comparison with the thermal models.

Thermal Models

The thermal models of Equation 1-5 are applied as a validation technique to the simulation results as well as determining the fundamental aspects of the simulation physics in terms of fluid phase and heat load. The main analysis is focused to evaluate the cooling effect (Equation 6) and to compare it with the boundary heat transfer of the simulations.

In principal, internal and external forced convection mechanisms occurs simultaneously as the coolant air flows into the cooling channel as well as over the surfaces of the stack. The total cooling effect is the summation of both cooling mechanisms. The evaluation of both cooling effects are based on the Newton's law of cooling,

$$Q = h A_s \Delta T \quad (1)$$

where A_s is the surface area exposed to the cooling fluid, ΔT is the temperature difference between the surface and the fluid, and h is the average heat transfer coefficient, determined from a dimensionless called the Nusselt number. The Nusselt number is based on the flow phase which is determined from the Reynolds number,

$$Re = \frac{V_m L_c}{\nu} \quad (2)$$

$$Nu = \frac{h L_c}{k} \quad (3)$$

Here, Re is the Reynolds number, the mean velocity, V_m , is normally taken as the incoming steady stream velocity, ν is the kinematic viscosity of the fluid, Pr refers to the Prandtl number of the fluid evaluated at the film temperature, and L_c is the characteristic length of the surface.

A suitable method to evaluate the internal forced convection cooling within the channels is by treating the channels as fins. Various geometrical parameters are to be determined for acquiring the estimated cooling channel efficiency, as well as determination of the logarithmic mean temperature difference across the channel. Determination of the Reynolds number within the channels also applies Equation 2, where L_c is replaced by the hydraulic diameter of the channel, D_h . The models presented can be referred in greater detail in [14].

$$Q = \bar{h} A_t \eta_o \theta_{LMTD} \quad (4)$$

The total cooling rate within the channels, Q , are related to the fin (channel) performance, η_o , the average heat transfer coefficient, \bar{h} , the total surface area of the cooling channels, A_t , and log mean temperature difference, θ_{LMTD} .

The average heat transfer coefficient is dependant on the Nusselt number, hydraulic diameter of the channel, D_h , and the conductivity of the fluid at a mean temperature. The Nusselt number is mainly influenced by the aspect ratio of the channel geometries and flow phase. The Nusselt numbers was determined as 7.54 for the single cooling channel and 3.27 for each of the 40 channels [15].

The evaluation of internal convection Reynolds number is an important step in ensuring analytical and simulation accuracy. Fluid streams with $Re < 2300$ are laminar. In this study, all the streams were evaluated based on its velocity and hydraulic diameter, and the internal flow was determined to be fully developed laminar flow for all cases.

For the log mean temperature difference, it is obtained using

$$\theta_{LMTD} = \frac{(T_s - T_{f,e}) - (T_s - T_{f,i})}{\ln \left[\frac{(T_s - T_{f,e})}{(T_s - T_{f,i})} \right]} \quad (5)$$

T_s refers to the surface temperature of the channels, while $T_{f,e}$ and $T_{f,i}$ are the exit and inlet fluid temperatures respectively.

The acquired cooling rates from the simulation are presented in terms of cooling performance, ε , which is a ratio indicating the simulated cooling effect against the given heat load (required cooling rate),

$$\varepsilon = \frac{\text{boundary heat transfer from simulation}}{\text{required cooling rate}} \times 100\% \quad (6)$$

Micro Cooling Channel Configurations

The reference fuel cell design for the work is the GASHUB 3 kW water-cooled PEM fuel cell system. The PEM fuel cell stack dimension is 365 mm length x 149.5 mm width x 239 mm height and consisting of 72 cells. Figure 2 shows a single bipolar plate geometry (excluding the reactant flow fields), integrated with cooling channels on its 5 mm thick surface, while Figure 3 shows the cell in a complete stack assembly.

Two micro cooling channel configurations of different numbers and geometries are investigated. The single channel and 40 channel configurations (refer Table 1 for specifications) are selected to compare the cooling effect of singular and multiple channels. Accounting for the land width (or gap) between channels that were fixed at 1 mm, the 40 channel configuration would give an aspect ratio of approximately 1.7. Based on Newton's law of cooling, a large convective cooling surface produces higher cooling effects. Furthermore, the cooling coefficient is related to the Nusselt number which in turn is dependant on the aspect ratio of the channel geometries. The single channel has a larger

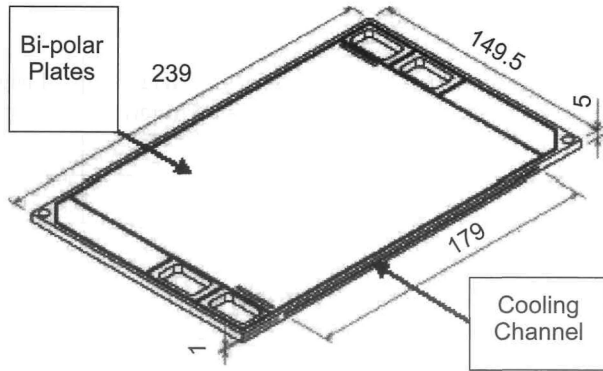


Figure 2: Single Bipolar Plate Geometry with Cooling Channels

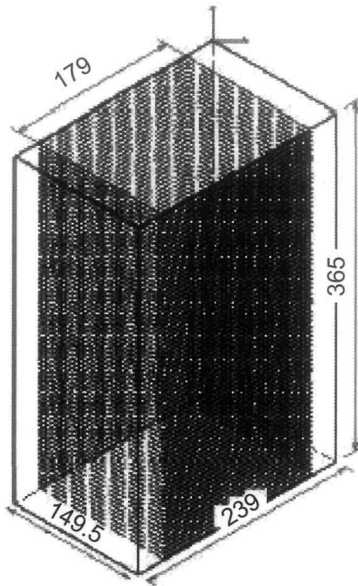


Figure 3: Stack Geometry with Imbedded Cooling Channels

aspect ratio (near unity) and twice the Nusselt number compared to the 40 channel configuration. However, the 40 channel configuration has the advantage of concentrated cooling rates and theoretically allows better cooling distribution across the bipolar plate than the single channel.

Table 1: Simulated Micro-channel Designs

Design label	Number of channels	Width (mm)	Height (mm)	Length (mm)
1. Ss1	1	179	2	150
2. Ms40	40	3.4	2	150

Simulation Cases and Parameters

The computational simulation was conducted using STAR-CCM Computational Fluid Dynamics (CFD) platform. Siegel [16] gave an in-depth review on the available CFD heat and mass transfer modeling specifically for PEM fuel cells. Though Park and Li [17] highlighted the penalties of CFD-based fuel cell models due to over-simplification and artificial boundary conditions, it should be noted here that this work applied only the standard CFD heat transfer models where a uniform heat load was pre-determined at a constant operating condition. This approach allows fast computing as local fuel cell operating conditions and electrochemical reactions are neglected.

The generated fuel cell heat is the maximum required cooling load to be continuously removed by the cooling fluid. The 72 cells, 3 kW PEM fuel cell stack has a rated voltage of 48 V. A PEM fuel cell normally operates at 50% conversion efficiency; thus, approximately 3 kW of heat would also be generated. To improve the investigation domain, the heat generation for the simulation was increased by lowering the conversion efficiency to 30%. This is equivalent to a thermal safety factor of 1.63 and a total stack cooling load of 4900 W, or 68 W of heat per plate.

In order to validate the simulation results and improve the depth of analysis, the cooling effects are simulated under different unit cases; a single plate unit case and an assembled stack unit case. Both cases are simulated under similar conditions. The major difference is that the single plate simulation only focuses on internal forced convection, while the stack simulation includes both internal and external forced convections, which is closer to practical conditions. Similar heat loads are applied to both cases. The parameter input values based on heat generation per volume (W/m^3) refers to their respective unit volumes.

Table 2 lists the boundary conditions applied for both simulation cases and Figure 4 displays the values of Reynolds number for each simulation cases. The internal and external flow Reynolds numbers are less than the critical values of 2300 and 500,000 respectively.

The actual fuel cell stack consists of 74 plates. In order to reduce computational power and simplify the heat flow, the stack was sketched as a block (neglecting the presence of MEA) imbedded with 74 arrays of micro

Table 2: Boundary Conditions and Parameters

Cooling Air		
Properties / parameters	Notes	Values
1. Flow phase	Laminar, with Re_{max} : • Internal flow, max • External flow, max	756 45,700
2. Flow source condition	Uniform inlet	50 mm from channel inlets
3. Inlet specifications	Velocity	1 m/s 2 m/s 3 m/s
4. Outlet specifications	Pressure outlet	1 atm
5. Inlet temperature	Ambient	30°C
6. Outlet temperature	Ambient	30°C
7. Inlet pressure	Ambient	1 atm
8. Outlet pressure	Ambient	1 atm
9. Thermal conductivity	Constant	0.02588 W/m.K
10. Specific heat, Cp	Constant	1005 J/kg.K
Bipolar plate/Stack		
Properties / parameters	Notes	Values
1. Material	Homogeneous	Carbon graphite
2. Specific heat [18]	Constant	710 J/kg.K
3. Density [18]	Constant	2240 kg/m ³
4. Thermal conductivity [19]	Constant	20 W/m.K
5. Cell efficiency (design rated)	At design safety factor of 1.63	30%
6. Projected heat generated	Steady and uniform	68 W (single plate) 4900 W (stack)
7. Projected heat flux	Steady and uniform	6044 W/m ³ (single plate) 441,195 W/m ³ (stack)

cooling channels. The stack was confined in an air cooling region, as illustrated in Figure 5.

Two regions of cooling air and plate/stack was assigned with an interface region defined at its contact surfaces. For the case of the plate, the interface region was defined within the cooling channels only (Figure 6). Therefore, the boundary heat transfer obtained at the interface from the simulation provides the internal convective cooling rates. For the stack case, the interface also covers the external stack surfaces, excluding the bottom stack surface which is defined as an adiabatic surface, allowing the total boundary heat transfer to be defined from the simulation analysis.

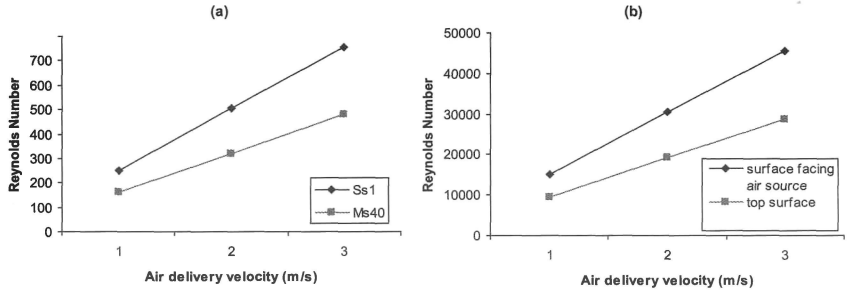


Figure 4: Reynolds Number at Simulated Air Velocities for (a) Internal Convection, and (b) External Convection

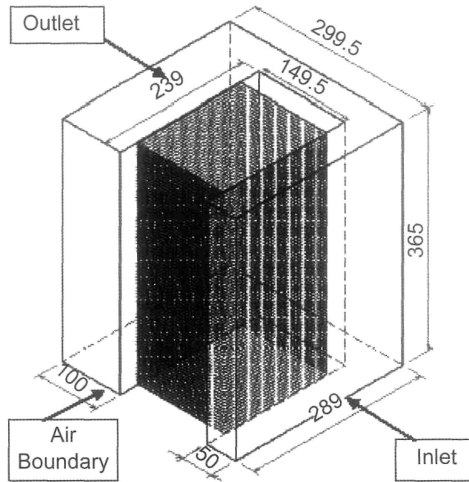


Figure 5: Stack and air Region Boundaries for the Stack Simulation Case

The selected physics models are three-dimensional analysis with ideal gas assumption, steady-state condition, laminar flow, segregated fluid temperature, segregated energy condition and stationary regions. Both air and plate regions were meshed with surface remesher, tetrahedral mesher and prism layer mesher.

The computational solution consists of iterative steps where a new value of temperature is issued from the precedent step of the computation. The main stopping criterion is achieving steady heat transfer conditions and thus the boundary heat transfer plots are continuously monitored (Figure 7). The normal range for convergence criterion is 10^{-1} to 10^{-4} , and convergence is generally accepted for a 0.1% variation in stack/plate temperature (in scalar value this is approximately a change of 0.05°C per iteration step). The computation of heat and flow involves the solution of the continuity, momentum and energy equations.

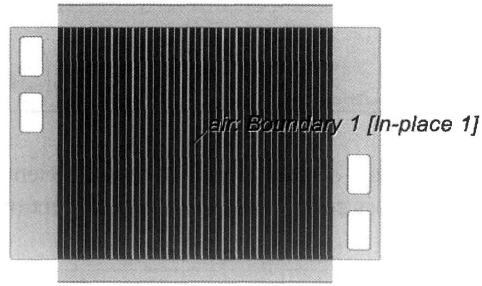


Figure 6: Interface Region for Plate Simulation Case

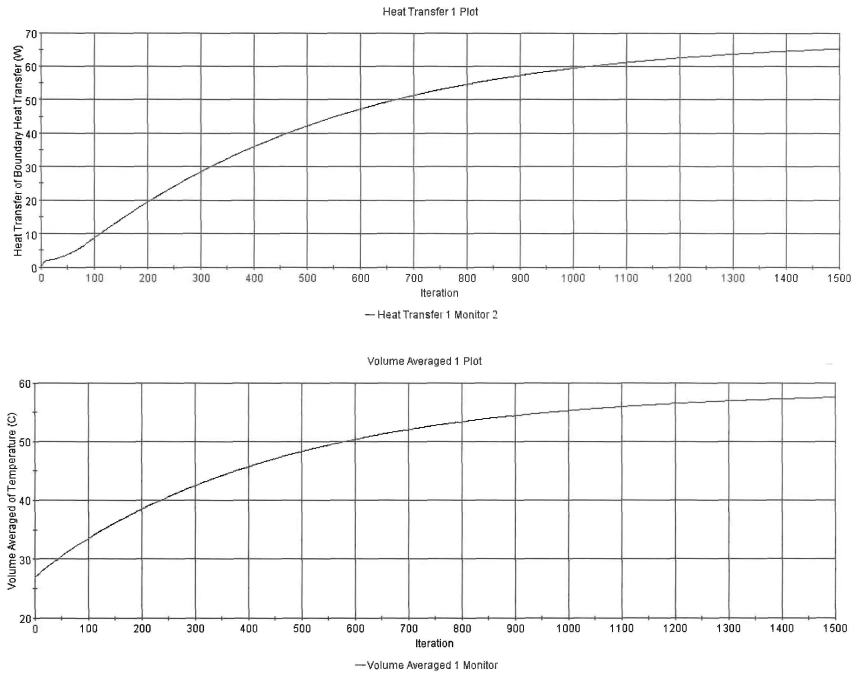


Figure 7: Computational Plot of Boundary Heat Transfer and Plate Temperature for the Single Channel at 3 m/s *

Continuity:

$$\iint_{boundaries} \rho u dA = 0$$

where ρ is the fluid density, u is the fluid velocity and A is the surface area of the channel.

Momentum:

$$\frac{d(\rho u A)}{dt} = \frac{dP \cdot A + \iint_{\text{boundaries}} \rho u^2 dA - 4c_f \frac{\rho u^2}{2} \frac{dx \cdot A}{D} - \xi \left(\frac{1}{2} \rho u^2 \right) A}{dx}$$

where P is the fluid pressure, c_f is the skin friction coefficient, D is the channel diameter, ξ the pressure loss coefficient, and x is the direction of flow.

Energy:

$$\frac{d(\rho e V)}{dt} = p \frac{dV}{dt} + \iint_{\text{boundaries}} \rho u H dA - hA(T - T_{\text{wall}})$$

where e is a measure of fluid internal energy per unit mass, V is the fluid volume, H is the total enthalpy, h denotes the convective heat transfer coefficient, and T is the temperature.

Results and Discussions

In order to systematically define the thermofluids behavior of the cooling cases, the simulation post-analyses are sectioned beginning with evaluation of the simulation methodology. Then, discussions on the temperature, air flow and pressure profiles are presented. The cooling effect and performance are thus analyzed accounting the thermofluids characteristics described in earlier analyses. Finally, validation of the simulation results is presented.

Evaluation of Simulation Methodology

To evaluate the simulation methodology reliability, a single plate simulation case on both cooling channel designs was also conducted under equivalent fluid and thermal conditions. The average stack/plate temperatures from the area-averaged and volume-averaged methods are presented in Figure 8. The R-mean square root statistical method was performed, and the standard deviation in terms of percentage difference from the stack simulation data is presented in Table 3.

All simulation showed less than 10% standard deviation values, even when data from both methods are combined and analyzed. The standard deviation for the volume-averaged temperature in both simulation cases is much lower than the area-averaged method, and rightfully should be the reference method for determining the average temperatures due to its higher repeatability. Consequently, this analysis confirms the reliability of the simulation methodology for this work.

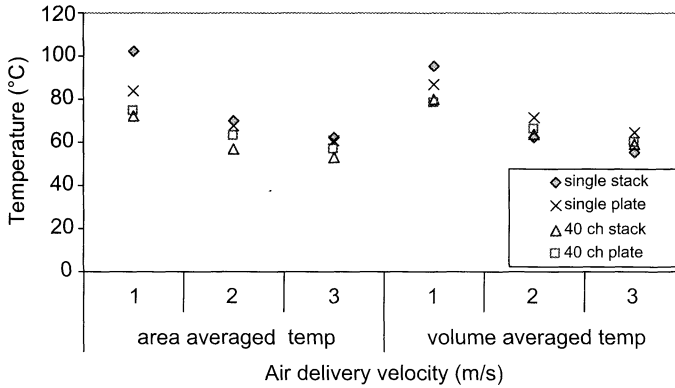


Figure 8: Area-averaged and Volume-averaged Plate/stack Temperatures

Table 3: Standard Deviation Values of the Average Stack/plate Temperature

Simulation case	Area-averaged method	Volume-averaged method	Combination
Single channel	7.5%	3.6%	6.5%
40 channel	2.9%	0.9%	3.4%

Thermofluids Characteristics

The volume averaged stack temperatures (also from Figure 8) indicates that the stack temperature does not change linearly with increasing inlet velocities. A significant temperature change occurred as the velocity changes from 1 m/s to 2 m/s; a 32°C drop for the single channel (from Reynolds number 250 to 500) and an 18°C drop for the 40 channels (from Reynolds number 160 to 320). The temperature change is much lower at 7°C and 4°C as the Reynolds number increased to 750 and 480 for the single and 40 channels respectively, leading to a conclusion that cooling with higher Reynolds number does not necessarily lead to a significant cooling effect. The coolant flow intensity selection should be dependant on the operational limit of the MEA. Based on these results, MEA with a lower temperature limit requires higher Reynolds number flows than those with higher temperature limits. For example, MEA operating at 60°C needs Reynolds number of 750 for the single channel and 480 for the 40 channels, while at elevated operating temperature of 80°C to 100°C, Reynolds numbers of 250 (single channel) and 160 (40 channels) are sufficient to maintain the stack temperature.

Figure 9 and 10 displays an example of the scalar temperature distribution on the surface of the plate and stack units at 3 m/s inlet velocity. As noted earlier, the coolest regions are located nearest to the coolant inlet plane, while the hottest regions are at the plate edges farthest from the inlet. The most significant behavior to note is the temperature distribution on the plate surface. The 40 channel configuration promotes a symmetrical surface temperature contour caused mainly by uniform cooling rates for the individual channels. The single channel, with a larger fluid flow region, promotes erratic flows and subsequently reduced cooling uniformity.

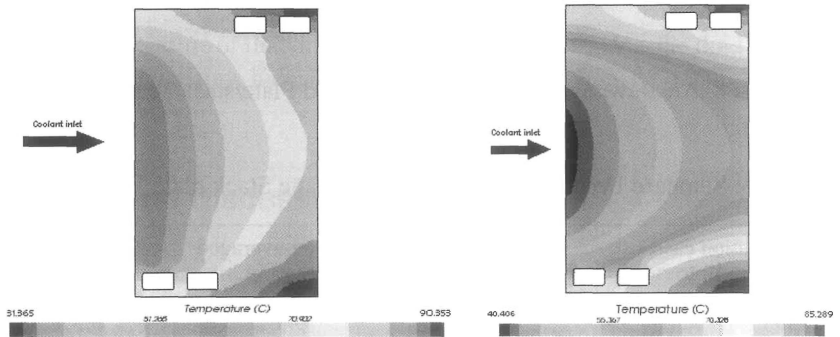


Figure 9: Temperature Contour of the Single Plate Case at 3 m/s Inlet Velocity for the Single Channel (left) and 40 Channel (right)

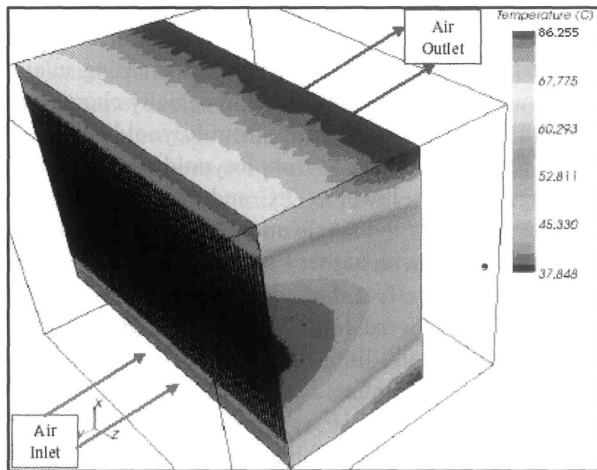


Figure 10: Temperature Profile of the 40 Channel Stack at 3 m/s

The plate average temperature profile across the sectional cross-sections (Figure 11) shows that temperature changes occur at an almost linear rate from the inlet, suggesting a reduced cooling rate along the channels. Improved cooling effects due to stack surface (exit plane) cooling was found at the 135 mm to 150 mm sections for all cases, leading to nearly constant exit temperatures. This effect is more dominant for the single channel than the 40 channels configuration. The exit plane temperature at 150 mm is 0.4°C to 1.4°C lower than the temperatures recorded at 135 mm plane section. This phenomenon could be related to possible backpressure flow as discussed in later in this paper.

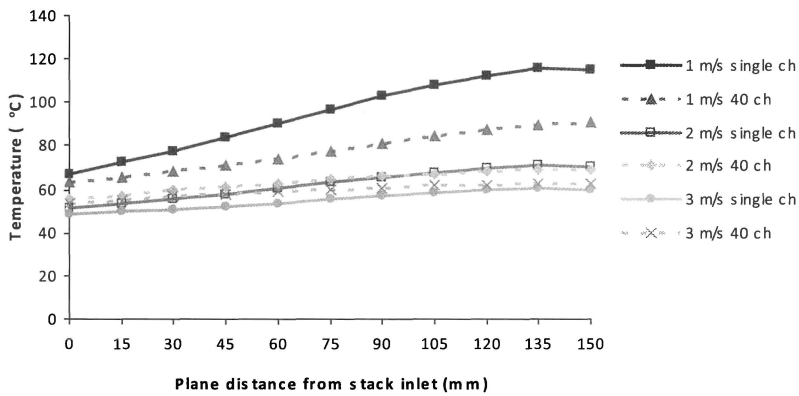


Figure 11: Stack Temperature Distribution at 15 mm Sections Normal to the Coolant Flow

The temperature non-uniformity in the stack was very high especially at low cooling velocities. The 40 channel configuration shows a lower temperature difference than the single channel for all cases. For the 40 channels, differences between the front and back surfaces of the stack (normal to coolant flow) is as high as 30°C at 1 m/s inlet velocity, and reduces to 15°C and 10°C as the inlet velocity increases to 2 m/s and 3 m/s.

By assuming a linear change along the stack, a linear stack temperature gradient was plotted in Figure 12. The linear temperature change rate was lowest (0.066 °C/mm gradient) for the 40 channels at 3 m/s, only slightly lower than registered at 2 m/s (0.1 °C/mm). Investigation by Adzakpa et al. [20] on an air-cooled PEM fuel cell similarly observed that the cooling intensity does not have a strong effect on the internal cell temperature gradient even though the average fuel cell temperature decreases.

PEM fuel cells are theoretically assumed to operate at a certain temperature. The reactivity of the gas diffusion layer and subsequent catalytic reactions are dependant on the localized temperature. Stack temperature uniformity is very much desirable, though almost impossible, thus a low temperature gradient is

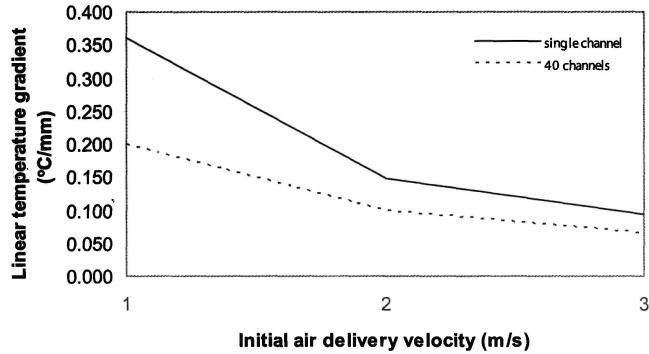


Figure 12: Linearized Stack Temperature Gradient

an important indicator to effective thermal management. From these simulation analyses, it is concluded for future reference works that plate temperature gradients of less than $0.1^{\circ}\text{C}/\text{mm}$ should be the minimal objective for any PEM fuel cell cooling configuration.

Figure 13 plots the air velocity distribution within the cooling channels. Velocity increase occurs immediately upon entry, and the 40 channels configuration shows a faster response to flow stability. A fully developed flow region theoretically allows a more effective cooling reaction to be achieved and is very desirable in convective cooling. Fully developed flows were achieved at approximately 15 mm from the inlet for the 40 channels, while the single channel achieved flow stability only at the 30 mm distance. The change in velocity also affects the flow Reynolds number. Figure 14 evaluates these changes based on the average velocities, and it was concluded that the flow throughout the channels are still in laminar flow phase. However, the single channel flow shows a larger inclination to reach transition flow phase as the inlet velocity increases to 3 m/s and higher.

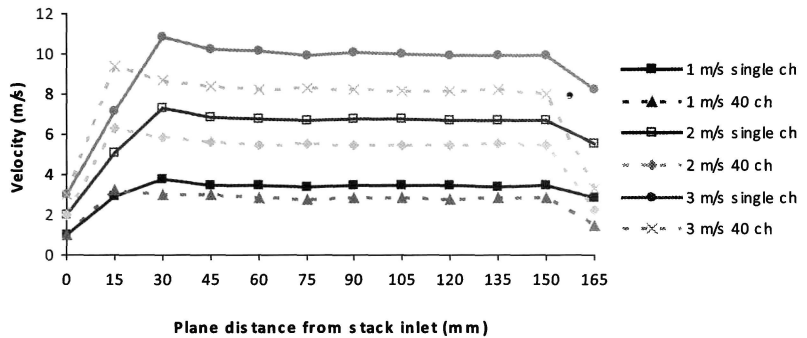


Figure 13: Air Velocity Gradients at 15 mm Plane Sections along the Channel

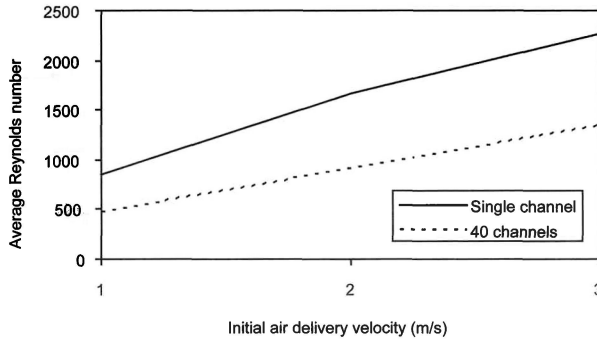


Figure 14: Reynolds Number Based on the Average Flow Velocity within the Channels

In Figure 15, the average velocity rise factor (AVRF) within the channels is introduced. This factor was evaluated by the ratio of the average air velocity flowing inside the channels to the nominal air delivery velocity. The AVRF for the single channel is 15% higher than the 40 channels, mainly due to the larger inlet area of the single channel that allows higher mass flow rates into the cooling channels. Higher AVRF subsequently results in higher heat transfer rates as shown by comparing the internal convection cooling between the channels at similar velocities. Generally, it is concluded that the air flow for the single channel is estimated to increase by approximately 330% from its initial delivery velocity while the 40 channels increases by 280%.

The air delivery and exit pressures were initially at the atmospheric condition of 101.32 kPa. Figure 16 and 17 illustrates the air pressure changes within the channels for the stack case simulation. At the channel entrance, air pressure was increased due to the inlet area resistance. The single channel, with a total inlet area of 0.02613 m² (or 30% larger), registers twice the pressure decrease

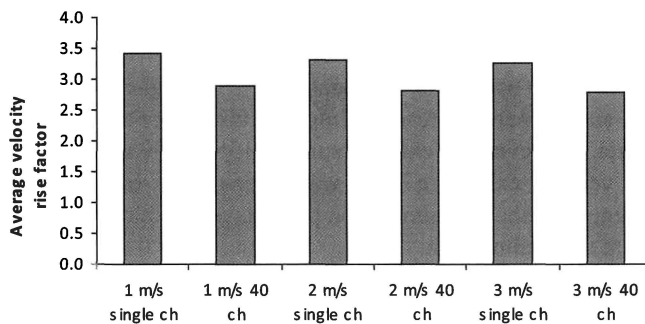


Figure 15: Comparison of Average Velocity Rise Factor from the Stack Simulation Case

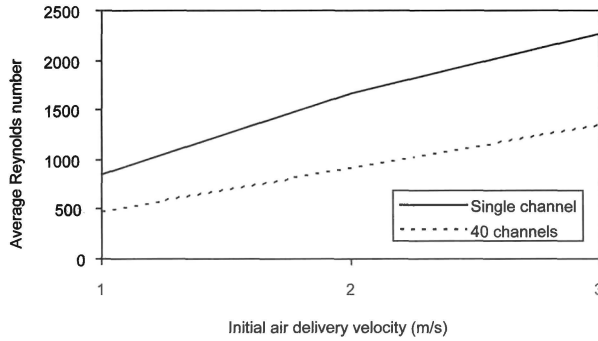


Figure 14: Reynolds Number Based on the Average Flow Velocity within the Channels

In Figure 15, the average velocity rise factor (AVRF) within the channels is introduced. This factor was evaluated by the ratio of the average air velocity flowing inside the channels to the nominal air delivery velocity. The AVRF for the single channel is 15% higher than the 40 channels, mainly due to the larger inlet area of the single channel that allows higher mass flow rates into the cooling channels. Higher AVRF subsequently results in higher heat transfer rates as shown by comparing the internal convection cooling between the channels at similar velocities. Generally, it is concluded that the air flow for the single channel is estimated to increase by approximately 330% from its initial delivery velocity while the 40 channels increases by 280%.

The air delivery and exit pressures were initially at the atmospheric condition of 101.32 kPa. Figure 16 and 17 illustrates the air pressure changes within the channels for the stack case simulation. At the channel entrance, air pressure was increased due to the inlet area resistance. The single channel, with a total inlet area of 0.02613 m² (or 30% larger), registers twice the pressure decrease

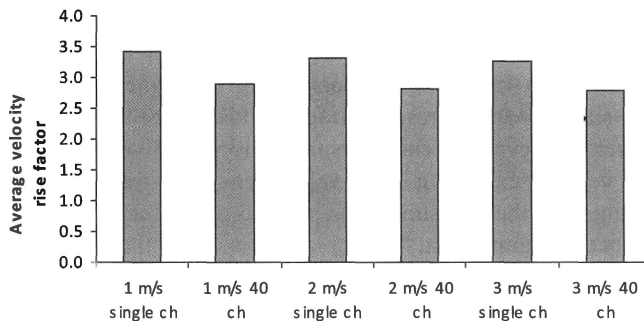


Figure 15: Comparison of Average Velocity Rise Factor from the Stack Simulation Case

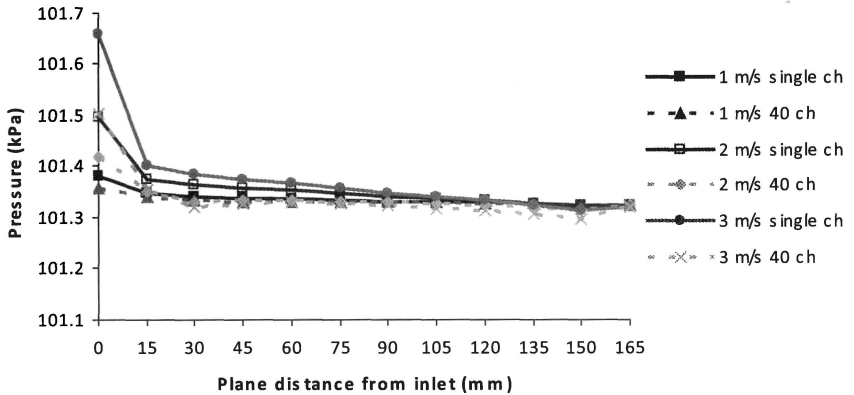


Figure 16: Air Pressure Distribution Inside the Cooling Channel at 15 mm Plane Sections

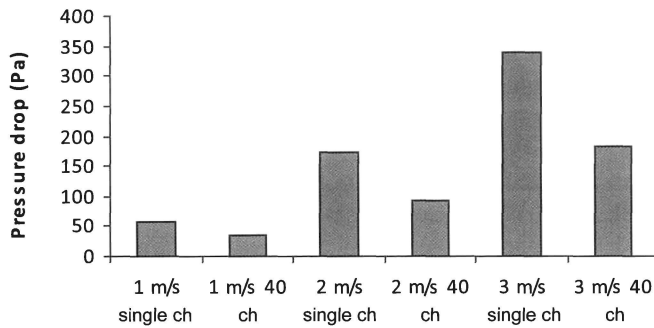


Figure 17: Analysis of Air Pressure Drop for the Simulated Cases

at similar delivery velocities compared to the 40 channels. The 40 channels configuration also allows a more uniform pressure gradient towards the exit. The highest pressure drop was fittingly expected from the highest delivery velocity, in which the single channel pressure drop was also twice the pressure drop of the 40 channel. However, the exit pressure (at 135 to 150 mm planes) of the 3 m/s delivery velocity exhibits a lower value than the surrounding atmospheric pressure, suggesting that the simulation predicts a possible backpressure flow could occur at the channel exit.

All simulation cases combining internal and external convection demonstrates the capability to achieve the required cooling performance of nearly 100%. However, the rates for internal cooling within the channels are varied. The internal convective cooling is constant with the flow velocity profile and AVRF. Higher velocities and mass flow allow rapid heat removal from the

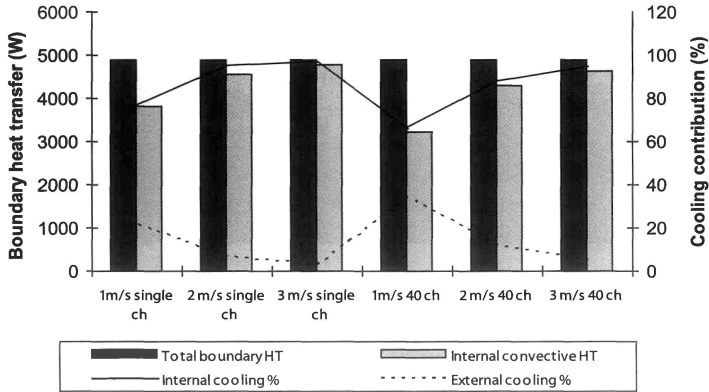


Figure 18: Cooling Rates and Contribution Percentages

hot surface. The 40 channel configuration demonstrates the lowest internal cooling percentage of 66% at 1 m/s. However, the slow moving air flow over the exposed stack surfaces allows the formation of flow boundary layers closer to the surface, providing adequate external convective cooling for a total cooling ratio of 100%. To achieve at least 90% internal convection effects, the minimum delivery velocity is determined to be 2 m/s (or $Re > 1000$).

The most important benefit of high internal cooling rates is the reduction of the temperature gradients throughout the bipolar plate. Comparing Figures 11, 12 and 18 indicates that higher internal cooling percentages, such as demonstrated by both designs at 3 m/s delivery velocity, leads to lower temperature gradients (less than $0.1^{\circ}\text{C}/\text{mm}$) and closer to uniform plate temperature distribution. Multiple cooling channel configurations are proven to be more suitable than a single channel in achieving low temperature gradients. Even though the internal cooling rate for the 40 channels at 1 m/s is lower than the single channel at similar delivery velocity, the average temperature gradient is 50% lower, resulting in better temperature distribution within the plate. Localized and concentrated cooling provided by the 40 channel configuration is effective in promoting fuel cell temperature uniformity. However, the optimum geometry and number of channels for this purpose is not explored further within this paper.

Validation with Analytical Models

Validation of the cooling rates was performed by comparing the internal convection boundary heat transfer from the simulation with analytical models on internal forced convection (Figure 19). The mean air velocity and average plate surface temperature for all analytical cases refers to the values obtained from the simulation. Assuming fully developed laminar flow throughout, the cooling channel and stack cooling rates were analyzed based on the fin efficiency

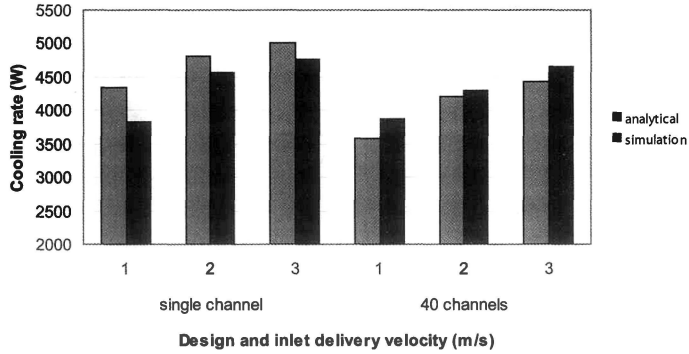


Figure 19: Analytical and Simulation Internal Convection Cooling Rates

analogy. The mean error is 8% for the single channel and 10% for the 40 channel, while the standard deviation is 4% and 9% for the cases respectively. The differences in cooling rate values are expected as the analytical models refer to a single velocity value throughout the channels. The margins of difference are acceptable, proving that the fin heat transfer analogy is applicable in predicting the internal convective cooling rates of a PEM fuel cell stack.

Overall, the analysis performed here based on thermofluid engineering principles allows a systematic approach in the evaluation of micro cooling channels designs of a PEM fuel cell stack. Cooling channel performance are generally evaluated based only on its maximum cooling effect, but a PEM fuel cell operation is dependant on temperature uniformity for optimum energy conversion. The analysis and discussions of the thermal conditions successfully identified the temperature gradients for each cooling cases. It is concluded that based solely on thermofluids analysis, the 40 channel configuration is a better option for application due to its lower stack temperature gradient as well as lower air pressure drop. Further investigation is currently undertaken to obtain the optimum geometry and number of channels for improved stack temperature distribution.

Conclusions

A CFD simulation analysis on a single channel and a 40 cooling channel configuration was conducted focusing on the thermofluids characteristics. The main parameter of concern was the cooling rates, where the PEM fuel cell stack was subjected to a constant predicted heat of 4900 W. From the combined effects of internal and external convections, the cooling performance of 100% was achievable for both configurations for Reynolds number as low as 200 for the 40 channel and 300 for the single channel. Stack temperature uniformity was improved when using multiple micro channels compared to a single wide

channel. Fluid flow analysis within the channels predicts that the AVRF for the single channel is 50% higher and the pressure decrease is twice as much. The simulation was also validated for its methodological reliability, and the internal convection cooling rates are within an acceptable margin of difference when compared with analytical heat transfer models. The analyses provided a detail computational design evaluation approach to optimize the air cooling channel configurations of a PEM fuel cell stack.

References

- [1] Bostic, E. (2004). "Fuel Cell Systems for the American Warfighter", *J. Fuel Cell Science and Technology* 1(1), 69-72.
- [2] Spiegel, C.S. (2007). *Designing and Building Fuel Cells*, McGraw-Hill New York, pp. 99.
- [3] van den Oosterkamp, P.F. (2006). "Critical issues in heat transfer for fuel cell systems", *Energy Conversion and Management* 47, 3552-3561.
- [4] Wen, C.Y. and Huang, G.W. (2008). "Application of a thermally conductive pyrolytic graphite sheet to thermal management of a PEM fuel cell", *J. Power Sources* 178(1), 132-140.
- [5] Bonville, L.J. Kunz, H.R., Song, Y., Mientek, A., Williams, M., Ching, A. and Fenton, J.M. (2005). "Development and demonstration of a higher temperature PEM fuel cell stack", *J. Power Sources* 144, 107-112.
- [6] Scholta, J., Messerschmidt, M., Jorissen, L. and Hartnig, Ch. (2009). "Externally cooled high temperature polymer electrolyte membrane fuel cell stack", *J. Power Sources* 190, 83-85.
- [7] Ju, H., Meng, H. and Wang, C.Y. (2005). "A single-phase, non-isothermal model for PEM fuel cells", *Int. J. Heat and Mass Transfer* 48, 1303-1315.
- [8] Wang, M., Guo, H. and Ma, C. (2006). "Temperature Distribution on the MEA surface of a PEMFC with a serpentine channel bed", *J. Power Sources* 157, 181-187.
- [9] Meyer, R.T. and Yao, B. (2006). "Control of a PEM fuel cell cooling system", Proceedings of IMECE2006, ASME Int. Mechanical Eng. Congress and Exposition.

- [10] Faghri, A. and Guo, Z. (2005). "Challenges and opportunities of thermal management issues related to fuel cell technology and modeling," *Int. J. Heat and Mass Transfer* 48, 3891-3920.
- [11] W.A. Najmi W. M. and Rahim, A. (2009). "Optimizing air cooling capability of polymer electrolyte membrane fuel cells through case-by-case cooling channel analysis", Proceedings of the Int. Conf. on Advances in Mechanical Engineering (ICAME), Malaysia.
- [12] Wen, C.Y., Lin, Y.S. and Lu, C.H. (2009). "Performance of a proton exchange membrane fuel cell stack with thermally conductive pyrolytic graphite sheets for thermal management", *J. Power Sources* 189, 1100-1105.
- [13] W.A. Najmi W. M., Rahim, A. and Azli, R. (2010) "Micro-channel optimization for an air-cooled polymer electrolyte membrane fuel cell by CFD simulation", Proceedings of the 3rd Engineering Conference on Advancement in Mechanical and Manufacturing for Sustainable Environment (EnCon), Malaysia.
- [14] Incropeca, F. P. and DeWitt, D. P. (2002). *Fundamentals of Heat and Mass Transfer Fifth Edition*, John Wiley and Sons, New Jersey, pp. 495-500.
- [15] Cengel, Y. (2003). *Heat Transfer A Practical Approach 2nd Int. Edition*, McGraw Hill, New York, pp. 437.
- [16] Siegel, C. (2008). "Review of computational heat and mass transfer modeling in polymer electrolyte membrane (PEM) fuel cells", *Energy* 33, 1331-1352.
- [17] Park, J. and Li, X. (2006). "Effect of flow and temperature distribution on the performance of a PEM fuel cell stack", *J. Power Sources* 162, 444-459.
- [18] Begot, S. and Kauffmann, J.M. (2009). "Estimation of internal fuel cell temperatures from surface temperature measurements", *J. Power Sources* 178, 316-322.
- [19] Dummery, L., Glises, R., Louahlia-Gualous, H. and Kaufmann, J.M. (2006). "Thermal management of a PEMFC stack by 3D nodal modeling", *J. Power Sources* 156, 78-84.
- [20] Adzakpa, K.P., Ramousse, J., Dube, Y., Akremi, H., Agbossou, K., Dostie, M., Poulin, A. and Fournier, M. (2008). "Transient air cooling thermal modeling of a PEM fuel cell", *J. Power Sources* 179, 164-176.